# Lattice Dynamics Simulation of Thermal Contraction of Faujasites

**ARTICLE** *in* THE JOURNAL OF PHYSICAL CHEMISTRY C · DECEMBER 2010

Impact Factor: 4.77 · DOI: 10.1021/jp1073736

# Lattice Dynamics Simulation of Thermal Contraction of Faujasites

**P. G. Krokidas,[†,‡] E. D. Skouras,[‡] V. Nikolakis,[‡] and V. N. Burganos*[,‡]**

*Department of Material Science, University of Patras, Greece, and Foundation for Research & Technology Hellas, Institute of Chemical Engineering & High Temperature Chemical Processes, Greece*

*Received: August 5, 2010; Revised Manuscript Received: October 22, 2010*

Negative coefficients of thermal expansion have been reported for certain zeolite structures, including LTA, NaX, and DAY, with immediate consequences on the mechanical stability and performance of the supported membranes in gas separations. This unusual behavior is typically attributed to the systematic rotation of the framework tetrahedrals that operate as rigid units. A new interatomic potential is proposed in this work and used in lattice dynamics calculations for the computation of the thermal expansion coefficient as well as of the elastic and bulk moduli of zeolite faujasite with different aluminum contents. Comparison of the present simulations with literature measurements as well as with experimental data carried out in this work showed that the dealuminated faujasite (DAY) crystals contract upon heating over the entire temperature range examined, whereas aluminosilicate NaX contracts up to the ambient temperature and then expands with increasing temperature. Our analysis showed that the effect of temperature on the faujasite unit cell volume depends on the rigidity of the $SiO_4$ and $AlO_4$ tetrahedra as well as on their ability to rotate around their corner sharing oxygen atoms.

## 1. Introduction

Knowledge of the zeolite thermal expansion coefficient is important to assess possible crack formation and/or grain boundary opening in supported polycrystalline zeolitic membranes. Such issues are crucial if a significant mismatch between the thermal expansion coefficient of the zeolitic membrane and the support exists, which might be detrimental for the membrane separation performance. Understanding of the mechanism underlying heat-induced contraction might also lead to the development of new smart materials with controlled axis expansion or zero coefficient of thermal expansion (CTE). Such characteristics are of interest in aerospace technologies,[1] microchips, fuel cells, optical devices,[2] etc.

Generally, the expansion of materials upon heating is attributed to the expansion of bond lengths; during heating the amplitude of vibrations along the bond axis increases, and the atoms, due to the asymmetry of the potential, feel an overall repulsive force. Thus, the time average distance ($r_0$) increases in order to achieve force equilibrium. In many materials, however, heating leads to contraction, characterized by a negative thermal expansion coefficient. Depending on the material, the origin of this behavior has been traced to different mechanisms, related to transverse vibrational modes, the libration phenomenon, phase transitions, and the mechanism of rigid unit modes (RUM). The latter is considered as the most probable cause of negative coefficients of thermal expansion (NCTE) in zeolites and involves modes of vibration that are observed in frameworks that are comprised of rigid polyhedra connected through sharing corners.[3] The corner-linked rigid polyhedrals (for instance, $SiO_4$) are able to rotate about the so-called "hinges" of the M−O−M type (Figure 1), where M are metal cations and O the oxygen atoms. In the case of zeolites, these hinges are the Si−O−Si and Al−O−Si bonds. In energy terms, the rotation about the M−O−M linkage is many times more favorable than the distortion of the polyhedra. These modes are of low frequency. Especially the rotative motion of these tetrahedra is referred to as a soft mode, due to its very low frequency. Dove et al.[4] carried out a geometrical analysis of the M−O−M rotations and derived a mathematical expression for the dependence of the expansion coefficient on the frequency of these modes of rotation

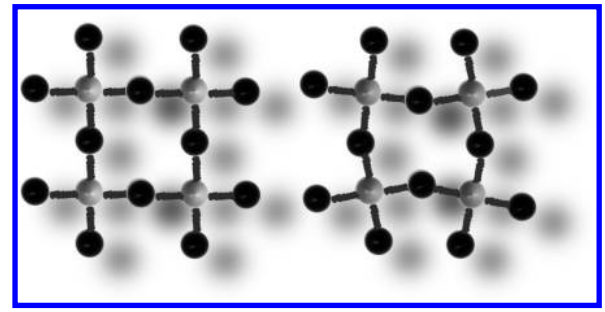

**Figure 1.** Schematic representation of the RUM mechanism, developing through the rotation of tetrahedra. M, gray spheres; O, black spheres.

$$a = -\eta_A \frac{k_B}{I\omega^2} \tag{1}$$

where $a$ stands for the expansion coefficient, $\eta_A$ is a geometrical coefficient, $k_B$ is Boltzmann's constant, $I$ is the moment of inertia of the rotating squares in a two-dimensional model, and $\omega$ is the frequency. According to eq 1, the magnitude of the negative expansion coefficient increases with decreasing frequency.

Moreover, contraction itself can also be considered as part of a mechanism that constitutes the response of materials upon heating. Generally, the mechanism of thermal expansion is the result of the anharmonicity of the forces acting between vibrating

* To whom correspondence should be addressed. E-mail: vbur@iceht.forth.gr.
† University of Patras.
‡ Institute of Chemical Engineering & High Temperature Chemical Processes.

10.1021/jp1073736 
Published on Web 12/03/2010

atoms that leads them to occupy more space as the amplitude of their motion increases. On the other hand, contraction through rotations of rigid units is compatible with geometric arguments. Heine et al.[5] suggested an equation that combines these two contributions

$$\gamma_{red} \approx -A + B\omega^2 \quad (2)$$

where $\gamma_{red}$ is a reduced Grüneisen parameter, $\omega$ is the frequency of the mode, and $A$ and $B$ are the geometrical and anharmonic constants, respectively. The Grüneisen parameter $\gamma$ is related to the coefficient of thermal expansion through $a = (C_v\gamma)/(3K)$, where $K$ is the bulk modulus and $C_v$ the heat capacity at constant volume. Equation 2 shows that the geometrical factor, $A$, which corresponds to the contribution of the rotations of the tetrahedra, is always negative, whereas the anharmonic part, $B$, contributes positively to expansion as the frequency increases. Moreover, it indicates that a small positive thermal expansion coefficient most probably results from combined contribution of both factors. Detailed information about all possible mechanisms of NTE can be found in the extensive reviews by Evans,[6] Barrera et al.,[7] and Miller et al.[8]

Examples of negative CTE in zeolites include ITQ-1, ITQ-3, and SSZ-23,[9] ITQ-4, IFR,[10,11] MFI,[12−15] LTA,[16] $AlPO_4$,[17] and FER.[18] Faujasite, which is studied in this work, is a zeolite that is often used in catalysis,[19−22] in adsorption,[23−25] and in ion exchange systems.[26] Depending on their Si to Al ratio, faujasites are called X (Si/Al between 1 and 2) and Y (Si/Al > 2) even though they both have topologically the same framework. Experiments[27] have shown that siliceous faujasite (DAY) exhibits NCTE from 25 K up to almost 600 K. These results agree with lattice dynamics calculations by Tschaufeser et al.,[16] who simulated the effect of temperature on the DAY unit cell volume. Couvest et al.[28] showed that the NaX unit cell contracts as temperature rises from 25 K to ambient. Measurements were not reported at elevated temperatures in that work; however, a single experimental point above room temperature indicates a change of sign of the CTE, implying that further heating could lead to expansion. The expansion of NaX has been verified by Noack et al.,[29] who carried out experiments between 423 and 723 K. In contrast to the case of DAY, simulations[16] failed to predict this experimental observation for NaX.

Despite the analysis of the simulation results for both NaX and DAY, the reason behind the nonmonotonic temperature dependence of the FAU thermal expansion coefficient still remains elusive. A possible explanation for the different thermal expansion behavior of NaX and DAY can be the presence of extraframework cations. The restricted motion of the tetrahedra or even the deformation of the rotating units that is imposed by the cations has been mentioned as tentative underlying mechanisms in the literature.[30,31]

The present work attempts to elucidate this issue and, more specifically, investigates the impact of Al and Na on the response of the faujasite framework upon temperature changes. A new potential is developed that can capture the effect of temperature on the faujasite unit cell volume over the entire range of Si/Al ratios ($1 < Si/Al < \infty$). Lattice dynamics calculations using the new potential are compared with experimental data and simulations using force fields from the literature and from this work. Analysis of the results and further simulations are carried out in order to understand the mechanism behind contraction or expansion upon heating. Finally, the capability of this new potential to predict the modulus of elasticity (Young modulus) and the bulk modulus of NaX crystals is examined.

## 2. Simulations

**2.1. Reconstruction of the Unit Cell.** The unit cells of DAY and NaX faujasites were initially reconstructed using literature data.[32,33] The unit cell of DAY belongs to the *Fd*3*m* space group, has a lattice constant of 24.8 Å, and consists of 384 oxygen atoms and 192 silicon atoms. The aluminosilicate NaX unit cell belongs to the *Fd*3 space group and has a lattice constant of 25.7 Å. Aluminum atoms replace part of the Si atoms, while Na ions are present at specific symmetric positions in order to preserve the neutral charge of the unit cell.

**2.2. Force Field Development.** A large number of potentials that describe siliceous compounds can be found in the literature. A widely used one is that developed by Catlow et al.[34] It consists of a Coulombic term for the electrostatic interactions, a Buckingham potential for the short-range interactions, and a three-body harmonic potential for the description of the O−Si−O and O−Al−O bond angle inside the tetrahedra. Oxygen polarizability is represented by the shell model.[35] The parameters of these terms have been obtained by fitting to the elastic properties of α-quartz. Recently, a new force field was presented by Ramsahye et al.[36] to simulate diffusion of chloroform inside NaY. Both potentials have parameters that explicitly distinguish the electrostatic and van der Waals interactions of Si and of Al atoms. The two most important differences between the two potentials are the following: (a) the potential by Ramsahye et al.[36] does not implement the core−shell model but treats the oxygen atoms as cores, like the rest of the atoms of the structure, and (b) the three-body harmonic potential for the bond angles O−Si−O and O−Al−O, in the case of Ramsahye et al.,[36] distinguishes between Si and Al atoms in contrast to the former potential,[34] which treats Si and Al sites similarly.

The intermolecular and the harmonic three-body terms are given by the following relations

$$V_r = A\exp(-r/\rho) - Cr^{-6} + \frac{q_1q_2}{r} \quad (3)$$

$$V_\theta = {}^1/_2K_\theta(\theta - \theta_0)^2 \quad (4)$$

where $V_r$ stands for nonbonded interactions, which are represented as a sum of Coulombic and van der Waals interactions, whereas $V_\theta$ is the three-body harmonic potential.

Both of these force fields were used in numerical simulations by the authors in order to study the temperature effect on DAY and NaX unit cells. The results showed that none of them could reproduce experimental data for the unit cell volume in a consistent manner for both DAY and NaX. In particular, the force field suggested by Catlow et al.[34] predicts the monotonic contraction of the DAY unit cell upon heating but cannot predict the expansion of the NaX unit cell above ambient temperature. On the other hand, the force field suggested by Ramsahye et al.[36] predicts successfully the switch from contraction to expansion in the case of the NaX unit cell but overpredicts the volume of the DAY unit cell and, at elevated temperatures, predicts expansion of DAY at variance with experimental data.

It is, thus, apparent that a new force field must be developed that can be applied to both DAY and NaX and can be, possibly, adopted to treat more zeolite types in the future.

The arguments that led to the new potential suggested in this work are as follows. It was found computationally that the value of the $K_\theta$ constant of the three-body harmonic potential of the intratetrahedral O−Si−O and O−Al−O bond angles plays a

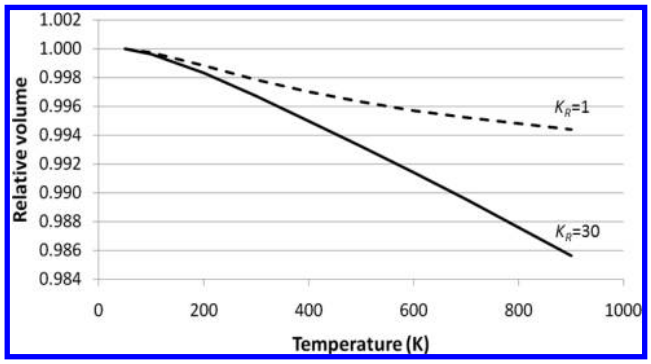


**Figure 2.** Dependence of the DAY unit cell volume on temperature for two $K_R$ values.

major role in the simulation of thermal response of the framework. Simulations of the temperature effect on a DAY unit cell by adjusting the value of $K_\theta$ showed that as the value of the constant increases the expansion is enhanced. This explains why the simulations using the force field of Ramsahye et al.[36] predict the expansion of the NaX unit cell in contrast to the simulations using the force field of Catlow et al.:[34] the same $K_\theta$ value ($K_\theta = 2.2$ eV/rad$^2$) for both O−Si−O and O−Al−O three-body potential is used in the latter case, whereas different $K_\theta$ values for the two bond angles are used in the former case. Specifically, a higher value ($K_\theta = 12.1$ eV/rad$^2$) is employed in the case of O−Si−O. This increased value, according to our simulation tests, introduces a factor that favors expansion. But, also, this higher value explains the reduced predictive capability of the potential by Ramsahye et al.[36] in the case of DAY simulations. The $K_\theta$ value is too high and contraction switches to expansion at elevated temperatures.

More generally, the adoption of a model that describes the rigidity of $MO_4$ tetrahedra with the use of the O−M−O intratetrahedral angles might lead to conclusions against physical intuition: as mentioned above, increased $K_\theta$ values of the intratetrahedral bond angles (O−M−O) favor expansion. If we accept that these angles describe the rigidity of the tetrahedra, then the above conclusion contradicts the RUM theory. Therefore, there is a need for a careful selection of the force field terms so that they facilitate the investigation of the mechanism behind the structural changes upon heating. Based on the above, the rigidity of the tetrahedra is described as follows: the hard interior of the tetrahedra is not described through the angle bond O−Si−O and O−Al−O as in previous attempts,[34,36] but with the use of harmonic bond terms for the Si−O and Al−O bonds, according to the following equations:

$$V_R^{Si-O} = {}^1/_2 K_R^{Si-O}(r - r_0^{Si-O})^2$$
$$V_R^{Al-O} = {}^1/_2 K_R^{Al-O}(r - r_0^{Al-O})^2 \quad (5)$$

In this way, it is possible to control the rigidity at a more fundamental level. The tetrahedra containing M−O bonds with lower $K_R$, such as $AlO_4$, will tend to deform, enhancing expansion. Indeed, simulations of the temperature effect on a DAY unit cell, where the $K_R$ of Si−O bond constant was adjusted, showed that as $K_R$ decreases, thermal contraction is less intensive (Figure 2). This is a consequence of the appropriate introduction of the $K_R$ term to the new potential. However, as the results imply, the rigidity alone cannot predict the expansion of the NaX unit cell above room temperature, even for high $K_R$ values. An additional term is needed to describe the change of the external angles of the tetrahedra. This is reasonable since, according to the RUM theory, the rotations of the rigid units are responsible for the contracting behavior. In the new potential, the ability of the tetrahedra to rotate and, hence, alter these external angles is described with the use of the harmonic potential of eq 6, for the Si−O−Si and Si−O−Al external bond angles.

$$V_\theta^{Si-O-Si} = {}^1/_2 K_\theta^{Si-O-Si}(\theta - \theta_0)^2$$
$$V_\theta^{Si-O-Al} = {}^1/_2 K_\theta^{Si-O-Al}(\theta - \theta_0)^2 \quad (6)$$

To understand the effect of the three-body potential constant $K_\theta$ on expansion, simulations were carried out by adjusting the value of the Si−O−Si angle $K_\theta$ constant. The results show that the contraction is limited or even switches to expansion as $K_\theta$ increases whereas it is enhanced as $K_\theta$ is reduced. This is also a meaningful observation since a decrease for $K_\theta$ of the intertetrahedral M−O−M bond angles results in more loosely joined tetrahedra that are more free to rotate and, in accord with the RUM mechanism, can cause contraction of the unit cell. In summary, the new potential involves eq 5 and eq 6, complemented by eq 3.

The values of the parameters of each term were found using the following procedure. Initial guesses for the harmonic potential of the Si−O bond and the three-body potential of the external bond angles Si−O−Si were taken from the cvff potential.[37] In the case of Al atoms, the corresponding harmonic bond potentials and the three-body harmonic potential terms were assigned initial values that result in a ratio of the order of 5, following similar ratio values reported in the literature.[36,38] Refinement of all the potentials terms to the initial structure[33] was made using the GULP program. The fit was carried out in a step-by-step procedure. First, refinement was applied to each Buckingham term separately, keeping the harmonic potential values equal to their initial values as mentioned above. Then, the harmonic bonding potential terms and the three-body harmonic potential terms were adjusted. Three iterations of this adjustment procedure were required for convergence. The final values are given in Table 1.

**2.3. Simulation of the Temperature Effect.** Most common numerical techniques for the simulation of structural changes involve lattice energy minimization. Relative atomic positions and lattice volume are optimized in order to minimize the static energy. The main disadvantage of this method is the absence of temperature effects, rendering it, thus, inefficient for the purpose of the present work. The effect of temperature can also be studied either by Monte Carlo or molecular dynamics. While they are efficient in specific problems, they also have two certain disadvantages. First, their accuracy is reduced at low temperatures, since they neglect the quantic character of vibrations and the finite motion at zero temperature. Second, the need to use ensemble averages introduces statistical uncertainty, which decreases upon increasing the square root of the domain length or the number of atoms used in the simulations.

In this work the lattice dynamics technique is employed. The effect of temperature is modeled by computing the vibrational frequencies of atoms in a periodic lattice. It uses a process similar to the lattice energy minimization; however, the quantity that is minimized is the Gibbs free energy

$$F = A + pV = E - TS + pV = E_{stat} + E_{vib} - TS + pV \quad (7)$$

**TABLE 1: Parameters of the Force Field Developed in This Work**

| | | long-range (Coulombic) potential | | | |
|---|---|---|---|---|---|
| | | Si | Al | O | Na |
| $q$ (e) | ref 34 | 4.0 | 3.0 | –2.0 | 1.0 |
| | ref 36 | 2.4 | 1.4 | –1.2 | 1.0 |
| | this work | 2.4 | 1.4 | –1.2 | 1.0 |
| | | short-range (Buckingham) potential | | | |
| | | Si–O | Al–O | O–O | Na–O |
| $A$ (eV) | ref 34 | 1283.907 | 1460.3 | 22764.3 | 5836.84 |
| | ref 36 | 30023.0 | 26998.0 | 894.6 | 8200.0 |
| | this work | 29856.8 | 27000.7 | 426.6 | 8199 |
| $\rho$ (Å) | ref 34 | 0.32052 | 0.29912 | 0.149 | 0.2387 |
| | ref 36 | 0.1621 | 0.1622 | 0.3244 | 0.218 |
| | this work | 0.1585 | 0.1622 | 0.3601 | 0.218 |
| $C$ (eV/Å$^6$) | ref 34 | 10.662 | 0.149 | 27.88 | 0 |
| | ref 36 | 12.84 | 12.84 | 0 | 11.8 |
| | this work | 12.765 | 12.873 | 0 | 11.8 |
| | | three-body harmonic potential | | | |
| | | O–Si–O | | O–Al–O | |
| $K_\theta$ (eV/rad$^2$) | ref 34 | 2.2 | | 2.2 | |
| | ref 36 | 12.1 | | 2.2 | |
| $\theta_0$ (deg) | refs 34, 36 | 109.47 | | 109.47 | |
| | | Si–O–Si | | Si–O–Al | |
| $K_\theta$ (eV/rad$^2$) | this work | 0.5 | | 1.35 | |
| $\theta_0$ (deg) | this work | 149.8 | | 149.8 | |
| | | harmonic bonding potential | | | |
| | | Si–O | | Al–O | |
| $K_R$ (eV/Å$^2$) | this work | 17 | | 3 | |
| $r_0$ (Å) | this work | 1.64 | | 1.76 | |

where $A$ is the Helmholtz free energy, $p$ and $V$ are the pressure and volume of the system, respectively, $E_{stat}$ and $E_{vib}$ are the static and vibrational parts of the energy of the system ($E$), $T$ is the temperature, and $S$ is the entropy of the system. The Gibbs free energy is the appropriate quantity that defines thermodynamic equilibrium at conditions of fixed pressure and temperature.

The Helmholtz free energy can be written as a sum over all modes and wavelengths of vibration:

$$A = \sum_{m,k}\left(\frac{1}{2}\hbar\omega(m,k) + k_B T \ln\left(1 - \exp\left(-\frac{\hbar\omega(m,k)}{k_B T}\right)\right)\right) \quad (8)$$

Before minimization, the dynamic matrix is constructed, which is the matrix of phonon frequencies of the lattice. It should be noted that the first derivative of the Helmholtz free energy is given by the following expression

$$\left(\frac{\partial A}{\partial \varepsilon'}\right)_{\varepsilon'',T} = \left(\frac{\partial E_{stat}}{\partial \varepsilon'}\right)_{\varepsilon''} + \sum_{m,k}\left[\frac{\hbar}{2\omega(m,k)}\left(\frac{1}{2} + \frac{1}{\exp\left(\frac{\hbar\omega}{k_B T}\right) - 1}\right)\left(\frac{\partial \omega^2}{\partial \varepsilon'}\right)_{\varepsilon''}\right] \quad (9)$$

where $\varepsilon$ stands for the set of the external and internal degrees of freedom (strains of the unit cell and atomic positions, respectively). $\varepsilon''$ denotes that all other degrees of freedom (but $\varepsilon'$) are kept constant.

Since frequencies are products of the second derivative of static energy, the calculation of the third derivative of static energy is required. The Newton−Raphson technique that is used for the minimization requires the second derivative of $A$ (Hessian). Because this is computationally expensive, the Hessian is calculated from the static energy, assuming that the Helmholtz free energy does not contribute significantly to the curvature. Further details about the technique and the GULP program that was employed in our work for the free energy calculations can be found in the work by Gale and Rohl.[39]

Lattice dynamics calculations can also be used for calculating the bulk and Young modulus of the crystals. In particular, the bulk modulus

$$K = -V\left(\frac{\partial P}{\partial V}\right) \quad (10)$$

is calculated from the Voight relation, which, in the case of a cubic crystal, is given from

$$K = \frac{1}{3}(C_{11} + 2C_{12}) \quad (11)$$

where $C_{ij}$ is ($ij$) element of the elastic constant matrix $C$ and is given by the second derivative of the static energy with respect to strain

$$C_{ij} = \frac{1}{V}\left(\frac{\partial^2 E_{static}}{\partial \varepsilon_i \partial \varepsilon_j}\right)_X \quad (12)$$

with $X$ denoting that the internal degrees of freedom (atom positions) are held constant.

The Young modulus is the ratio of the tensile stress in direction $i$ to the tensile strain, $Y = \sigma_i/\varepsilon_i$, in the same direction and can be calculated from

$$Y_i = S_{ii}^{-1} \quad (13)$$

where $S_{ij}$ is the elastic compliance and is produced by inverting the elastic constant matrix, $C_{ij}$.

**2.4. Experimental Section.** Powder X-ray diffraction of FAU crystals (of the NaX type) in controlled atmosphere was carried out as a function of temperature (323−673 K) using a Brücker D8 Advanced diffractometer equipped with a Lynx Eye detector using CuKα radiation. The powder samples were placed in an Antoon Paar XRK-900 high temperature reactor chamber and were degassed at 400 °C in vacuum. The patterns were recorded in the $2\theta$ range of 5−55° at a scan step of 0.02 and a scan speed of 5 s per step. At each temperature, the sample stage was realigned in order to take into account the vertical shift of the surface due to thermal expansion. The unit cell size was then estimated using the following procedure. The first 15 peaks of each pattern were indexed in order to get a first approximation of the unit cell size at each temperature. This value was used as starting point of the refinement process that was carried out using the Le Bail method[40] and the GSAS package.[41] This approach is based on the Reitveld refinement technique[42] but has the advantage that no prior knowledge of the structure is needed.

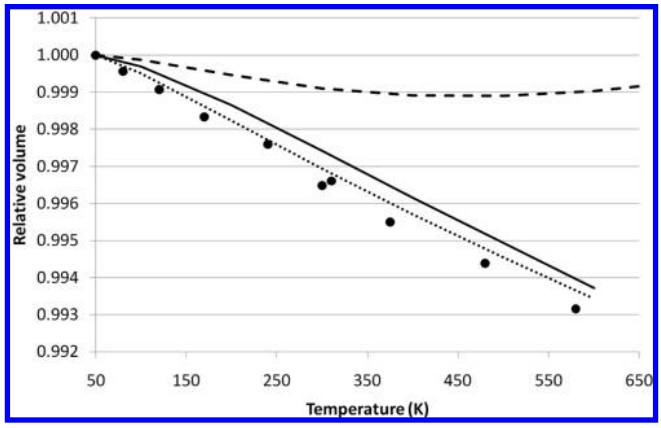


**Figure 3.** Experimental (points) and calculated (curves) relative unit cell volume for DAY. •••, potential from ref 34; ---, potential from ref 36; —, new potential (this work).

## 3. Results and Discussion

The experimental data for the effect of heating on the DAY unit cell volume from literature[27] are compared with calculations using the three force fields in Figure 3. Simulations using the potential of Catlow et al.[34] reproduce the monotonic contraction of the DAY unit cell. On the other hand, the potential of Ramsahye et al.[36] cannot predict the actual unit cell contraction, overestimates the volume, and predicts expansion above 400 K. On the contrary, simulations with the new potential that is suggested here reproduce the experimental points over the entire temperature range.

Figure 4 shows experimental and computational results for NaX faujasite. The crystals that were used in the temperature range 50−320 K[28] had Si/Al ∼ 1.5, whereas crystals in the range 320−700 K had Si/Al ∼ 1.16. These ratios were taken into account in the reconstruction of the unit cells that were subsequently used in the thermal response simulations. Experimental data from literature (Figure 4a) show that NaX contracts up to the ambient temperature, while experimental data of this work (Figure 4b) show that further increase of the temperature above ambient results in an increase of the unit cell size. Furthermore, the unit cell parameters of all experimental and simulation data are shown in Table 2. This confirms that faujasite has a thermal expansion coefficient with temperature dependent sign. Our simulations using the potential of Catlow et al.[34] could not reproduce the unit cell changes over the temperature range examined here. On the other hand, simulations using the potential of Ramsahye et al.[36] yield very good results and successfully predict both the contraction and the expansion upon heating. Simulations using the new force field reproduce the NaX contraction below ambient temperature, predict the minimum of the unit cell volume around room temperature, and follow the expansion above it. Despite some small deviation at temperatures higher than the ambient, it can be safely stated that the new potential is applicable to faujasites of different Si/Al ratios over a broad temperature range.

The conclusion of the above results is that none of the two potentials found in the literature could reproduce for both faujasite types examined here (DAY and NaX) the actual dependence of the unit cell volume on temperature. On the other hand, the results obtained with the new potential suggested in this work show a very good agreement in both faujasite types below and above the ambient temperature.

The same simulation tools can be used for the investigation of the mechanism behind the peculiar thermal response of FAU. The four Si−O−Si and Si−O−Al bond angles around the Si and Al sites were calculated as functions of temperature. The angles that affect the size of the 12-member rings were denoted as 1 and 2, and the angles that affect the diameter of the double 6-member rings as 2 and 4 (Figure 5). The four angles have different values but the same temperature dependence. Thus, for simplicity we decided to compare the unit cell change of DAY and NaX to the corresponding average change of the four angles (Figure 6). It is clear that the volume change (Figure 6a) for both DAY and NaX is similar to the change of the external angles (Figure 6b). In the case of DAY, all angles shrink monotonically upon heating. In the case of NaX, shrinkage of the bond angles takes place only at temperatures less than the ambient one. At room temperature the bond angles reach a minimum and then increase with temperature. A similar experimental observation is reported in the work of Bull et al.,[18] where expansion of the *Pnnm* phase of calcined siliceous ferrierite is noted as a result of the opening of the Si−O−Si bond angles. This minimum in the Si−O−Al bond angle can be attributed to the value of $K_\theta^{\mathrm{Si-O-Al}}$ of the three-body harmonic potential (eq 6) which is 2.7 times higher than that of $K_\theta^{\mathrm{Si-O-Si}}$. The difference between these values probably captures the difficulty of the Si−O−Al angle rotation due to the presence of $Na^+$. Similar arguments have been expressed in the literature,[13] to explain the differences between CTE of Al-containing HZSM-5 and that of pure siliceous ZSM-5. These results clearly indicate that the observed changes of the unit cell volume with temperature are related to the rotation of the rigid units (tetrahedra).

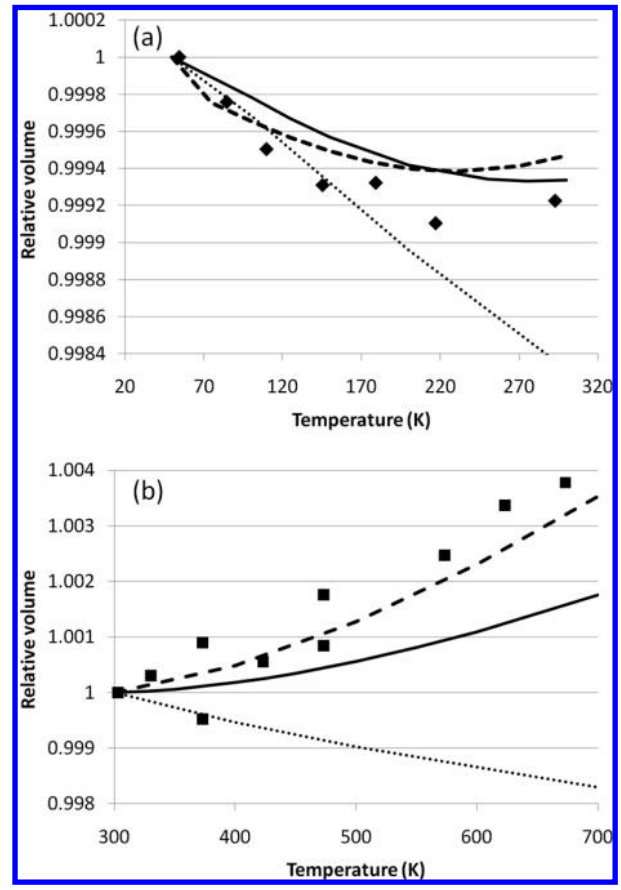


**Figure 4.** Experimental (points) and calculated (curves) relative unit cell volume for NaX: between (a) 50 and 320 K, Si/Al = 1.5; (b) 320 and 600 K, Si/Al = 1.15. •••, potential from ref 34; ---, potential from ref 36; —, new potential (this work).

Additionally, the Si−O and Al−O bond length and the O−Si−O and O−Al−O bond angle changes upon heating were

**TABLE 2: Comparison of Experimental and Calculated Lattice Constant of DAY and NaX Crystals at Different Temperatures**

| | DAY | | | | |
|---|---|---|---|---|---|
| | simulations using force field from | | | experiments | |
| | this work | ref 36 | ref 34 | ref 27 | |
| $T$ (K) | $a$ (Å) | $a$ (Å) | $a$ (Å) | $T$ (K) | $a$ (Å) |
| 50 | 24.5618 | 24.7150 | 24.2946 | 50 | 24.2735 |
| 100 | 24.5593 | 24.7131 | 24.2908 | 120 | 24.266 |
| 200 | 24.5508 | 24.7069 | 24.2804 | 170 | 24.26 |
| 300 | 24.5407 | 24.6979 | 24.2695 | 300 | 24.245 |
| 400 | 24.5303 | 24.6954 | 24.2593 | 375 | 24.237 |
| 500 | 24.5201 | 24.6915 | 24.2494 | 480 | 24.228 |
| NaX (Si/Al = 1.5) | | | | | |
| | simulations using force field from | | | experiments | |
| | this work | ref 36 | ref 34 | ref 28 | |
| $T$ (K) | $a$ (Å) | $a$ (Å) | $a$ (Å) | $T$ (K) | $a$ (Å) |
| 50 | 25.1143 | 25.0680 | 25.0605 | 54.6 | 24.8062 |
| 100 | 25.1125 | 25.0654 | 25.0579 | 109.9 | 24.8021 |
| 200 | 25.1094 | 25.0622 | 25.0519 | 217.2 | 24.7988 |
| 300 | 25.1088 | 25.0630 | 25.0465 | 293 | 24.7998 |
| NaX (Si/Al = 1.15) | | | | | |
| | simulations using force field from | | | experiments | |
| | this work | ref 36 | ref 34 | this work | |
| $T$ (K) | $a$ (Å) | $a$ (Å) | $a$ (Å) | $T$ (K) | $a$ (Å) |
| 400 | 25.1053 | 25.0630 | 25.0390 | 423.15 | 25.1763 |
| 500 | 25.1085 | 25.0696 | 25.0353 | 473.15 | 25.1864 |
| 600 | 25.1129 | 25.0782 | | 573.15 | 25.1923 |

determined. The analysis of the results for the DAY showed that the Si−O bond length and the O−Si−O bond angles remain unchanged upon heating, which means that the $SiO_4$ tetrahedra shape is not affected by temperature. Thus, DAY behaves as a system of rigid polyhedra, with unchanged inner bonds and loose external angles that are able to rotate around their hinges. A similar observation about the response of the DAY unit cell upon heating has been made in the literature.[27]

In the case of NaX, the Al−O bond length increases by about 0.005%, which is 1 order of magnitude lower than the volume change. This can be attributed to the value of $K_R^{Al-O}$ of the harmonic bonding potential (eq 5) which is nearly 5.7 times lower than $K_R^{Si-O}$. Thus, in the case of aluminosilicate FAU, there is a number of tetrahedra that are less rigid because $K_R^{Al-O} < K_R^{Si-O}$ and their rotation about the oxygen hinges is restricted by the presence of the extraframework cations. The O−Al−O bond angles remained constant upon heating, indicating that the $AlO_4$ tetrahedra are also rigid units.

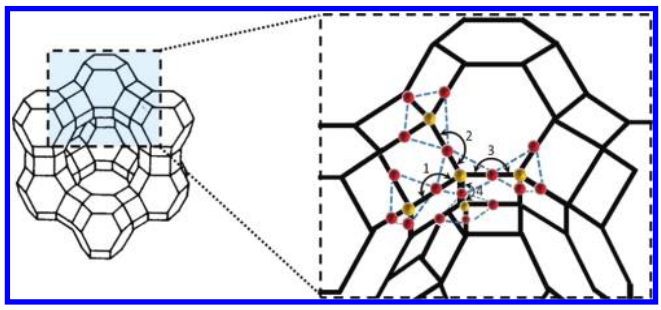


**Figure 5.** FAU unit cell showing the angles 1−4 between $SiO_4$ tetrahedra.

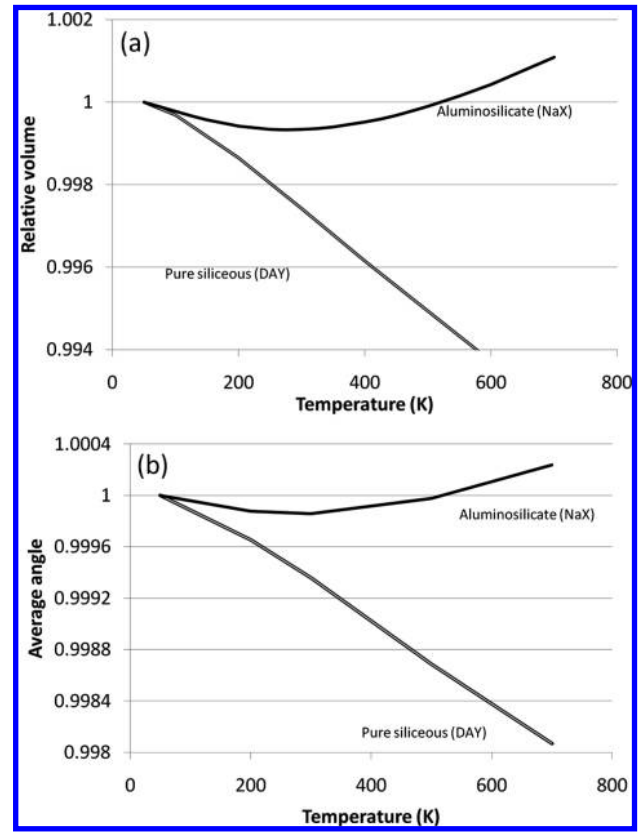


**Figure 6.** (a) Volume change and (b) average change of all four angles for pure siliceous and aluminosilicate NaX unit cell, upon heating.

While in the case of DAY the contractive mechanism of rigid tetrahedra rotation is dominant, in the case of NaX two competitive mechanisms develop. At low temperatures, just like in DAY, the unit cell contracts upon heating. At room temperature the negative and positive (as described in the previous paragraph) thermal expansion mechanisms contribute equally, and the volume goes through a minimum. As the temperature rises, the effect of the Al and $Na^+$ presence dominates and the angles open up, resulting in expansion of the unit cell of NaX.

In addition to the effect of temperature on unit cell volume, the new potential is used also for the calculation of certain mechanical properties of the faujasite, namely, the Young and bulk moduli. Both of these parameters reflect the deformation of the crystal lattice due to the application of isotropic or axial stresses. These quantities are based on second-order derivatives of the energy, and, hence, a successful calculation of them is expected to reflect the reliability of the force field developed in this work. In addition to the thermal expansion coefficient, these properties are also important in the field of zeolite membrane science, since zeolite membranes experience stresses due to the interface with the support or due to adsorption that tend to deform them and might create defects. Thus, knowledge of these properties is also of great interest.

To test the ability of the new force field to predict negative CTE in other zeolite structures, we simulated the effect of temperature on the siliceous orthorhombic framework of MFI,[43] which is known to contract upon heating.[44,45] The unit cell parameters estimated from our simulations are compared to the experimental data from the literature[45] in Table 3. It can be seen that simulations predict correctly the unit cell contraction upon heating in contrast with previous attempts[46] which predict expansion up to 600 K (using lattice dynamics and the force

**TABLE 3: Comparison of Experimental and Calculated Lattice Constants of MFI Crystals at Different Temperatures**

| | simulations | | | experiments[44] | | |
|---|---|---|---|---|---|---|
| $T$ (K) | $a$ (Å) | $b$ (Å) | $c$ (Å) | $a$ (Å) | $b$ (Å) | $c$ (Å) |
| 375 | 20.0243 | 19.9119 | 13.3701 | 20.0880 | 19.8750 | 13.3820 |
| 475 | 20.0194 | 19.9033 | 13.3596 | 20.0830 | 19.8820 | 13.3800 |
| 575 | 20.0145 | 19.8943 | 13.3487 | 20.0730 | 19.8760 | 13.3760 |
| 725 | 20.0076 | 19.8797 | 13.3319 | 20.0590 | 19.8700 | 13.3700 |
| 775 | 20.0056 | 19.8743 | 13.3260 | 20.0550 | 19.8680 | 13.3680 |

**TABLE 4: Experimental and Calculated Values of Young and Bulk Moduli for the NaX Crystals**

| simulations with potential from | $Y$ (GPa) | $K$ (GPa) |
|---|---|---|
| ref 34 | 41 | 57.2 |
| ref 36 | 50 | 52.8 |
| this work | 30 | 50.3 |
| experiments | $38.7 \pm 1.7$[46] | 35.2[47] |

field of Catlow et al.).[34] The deviation between the simulated and measured absolute values of the unit cell constants might be due to the pentasil units in MFI structure. These units consist of eight five-member rings and are not present in FAU. Accurate description of these units with a force field requires, probably, further adjustments and optimizations of the force field parameters.

The Young and bulk moduli were calculated using the two potentials from the literature and the new potential suggested in this work. The calculation of Young and bulk moduli was carried out with the use of the second-order derivatives of the energy with respect to strain according to eq 12, according to eq 11 and eq 13, respectively. The effect of the choice of the interatomic potential on the elastic properties is shown in Table 4. Note that the calculated value of Young modulus significantly depends on which potential is used in the simulations. Despite the differences between the calculated values, in all cases the Young modulus predictions are close to the value reported for NaX films.[47] On the other hand, the bulk modulus for NaX crystals predicted by all three force fields differ by only ~14%. All these values are higher than the bulk modulus of NaX estimated from high pressure synchrotron X-ray measurements using silicon oil as pressure transmitting medium.[48] Understanding of the phenomena that underlie the effect of pressure or strain in zeolite unit cell volume requires further investigation. This work is in progress by the authors.

## 4. Conclusions

Experiments reported in the literature[16] but also carried out in this work show that NaX faujasite contracts upon heating below room temperature and expands above it. In contrast, the unit cell of DAY contracts all over the entire temperature range of the experiments.[27] A new potential is developed that is based on a previous one from the literature[36] but takes into account both the rigidity of the tetrahedra and the stiffness of their external angles. The new potential can be adopted successfully for both DAY and NaX crystals. Lattice dynamics simulations showed that the predicted changes of the unit cell volumes are in very good agreement with the experimental results for both faujasite compositions. The analysis of the simulation results shows that in agreement with the RUM theory, the rotations of the tetrahedra are responsible for the unit cell volume changes with temperature. Further simulations showed that the presence of both Al and $Na^+$ affects the thermal response of the structure: The Al−O bonds being longer and softer result in less rigid tetrahedra, which tend to deform upon heating, while the Na cations constrain the rotations of the tetrahedra.

## References and Notes


(1) Imanaka, N.; Hiraiwa, M.; Adachi, G.; Dabkowska, H.; Dabkowski, A. *J. Cryst. Growth* **2000**, *220*, 176–179.

(2) Closmann, C.; Sleight, A. W. *J. Solid State Chem.* **1998**, *139*, 424–426.

(3) Giddy, A. P.; Dove, M. T.; Pawley, G. S.; Heine, V. *Acta Crystallogr.* **1993**, *49*, 697–703.

(4) Welche, P. R. L.; Heine, V.; Dove, M. T. *Phys. Chem. Miner.* **1998**, *26*, 63–77.

(5) Heine, V.; Patrick, R. L.; Dove, W. M. T. *J. Am. Ceram. Soc.* **1999**, *82*, 1793–1802.

(6) Evans, J. S. O. *J. Chem. Soc.* **1999**, 3317–3326.

(7) Barrera, G. D.; Bruno, J. A.; Barron, T. H. K.; Allan, N. L. *J. Phys.: Condens. Matter* **2005**, *17*, 217–252.

(8) Miller, W.; Smith, C. W.; Mackenzie, D. S.; Evans, K. E. *J. Mater. Sci.* **2009**, *44*, 5441–5451.

(9) Li, J.; Yokochi, A.; Amos, T. G.; Sleight, A. W. *Chem. Mater.* **2002**, *14*, 2602–2606.

(10) Woodcock, D. A.; Lightfoot, P.; Wright, P. A.; Villaescusa, L. A.; Diaz-Cabanas, M. J.; Camblor, M. A. *J. Mater. Chem.* **1999**, *9*, 349–351.

(11) Woodcock, D. A.; Lightfoot, P.; Villaescusa, L. A.; Dıaz-Cabanas, M. J.; Camblor, M. A.; Engberg, D. *Chem. Mater.* **1999**, *11*, 2508–2514.

(12) Park, S. H.; Groβe-Kunstleve, R. W.; Graetsch, H.; Gies, H. *Progress in Zeolite and Microporous Materials*; Studies in Surface Science and Catalysis; Elsevier: Amsterdam, 1997.

(13) Marinkovic, B. A.; Jardim, P. M.; Rizzo, F.; Saavedra, A.; Lau, L. Y.; Suard, E. *Microporous Mesoporous Mater.* **2008**, *111*, 110–116.

(14) Bhange, D. S.; Ramaswamy, V. *Microporous Mesoporous Mater.* **2007**, *103*, 235–242.

(15) Marinkovic, B. A.; Jardim, P. M.; Saavedra, A.; Lau, L. Y.; Baehtz, C.; de Avillez, R. R.; Rizzo, F. *Microporous Mesoporous Mater.* **2009**, *71*, 117–124.

(16) Tschaufeser, P.; Parker, S. C. *J. Phys. Chem.* **1995**, *99*, 10609–10615.

(17) Attfield, M. P.; Sleight, A. W. *Chem. Mater.* **1998**, *10*, 2013–2016.

(18) Bull, I.; Lightfoot, P.; Villaescusa, L. A.; Bull, L. M.; Gover, R. K. B.; Evans, J. S. O.; Morris, R. E. *J. Am. Chem. Soc.* **2003**, *125*, 4342–4349.

(19) Degnan, T. F., Jr. *Top. Catal.* **2000**, *13*, 349–356.

(20) Marcilly, C. *J. Catal.* **2003**, *216*, 47–62.

(21) Marcilly, C. *J. Catal.* **2000**, *13*, 357–366.

(22) Xavier, N. M.; Lucas, S. D.; Rauter, A. P. *J. Mol. Catal. A: Chem.* **2009**, *305*, 84–89.

(23) Coronas, J.; Noble, R. D.; Falconer, J. L. *Ind. Eng. Chem. Res.* **1998**, *37*, 166–176.

(24) Noack, M.; Kölsch, P.; Venzke, D.; Toussaint, P.; Caro, J. *Microporous Mater.* **1994**, *3*, 201–206.

(25) Coronas, J.; Falconer, J. L.; Noble, R. D. *AIChE J.* **1997**, *43*, 1797–1812.

(26) Walton, K. S.; Abney, M. B.; LeVan, M. D. *Microporous Mesoporous Mater.* **2006**, *91*, 78–84.

(27) Attfield, M. P.; Sleight, A. W. *Chem. Commun.* **1998**, *5*, 601–602.

(28) Couvest, J. W.; Jones, R. H.; Parker, S. C.; Tschaufeser, P.; Catlow, C. R. A. *; J. Phys.: Condens. Matter* **1993**, *5*, 329–332.

(29) Noack, M.; Schneider, M.; Dittmar, A.; Georgi, G.; Caro, J. *Microporous Mesoporous Mater.* **2009**, *117*, 10–21.

(30) Gatt, R.; Zammit, V.; Caruana, C.; Grima, J. N. *Phys. Status Solidi B* **2008**, *245*, 502–510.

(31) Williams, J. J.; Smith, C. W.; Evans, K. E.; Lethbridge, Z. A. D.; Walton, R. I. *Chem. Mater.* **2007**, *19*, 2423–2434.

(32) Fitch, A. N.; Jobic, H.; Renouprez, A. *J. Phys. Chem. B* **1986**, *90*, 1311–1318.

(33) Vitale, G.; Mellot, C. F.; Bull, L. M.; Cheetham, A. K. *J. Phys. Chem. B* **1997**, *101*, 4559–4564.

(34) Catlow, C. R. A.; Freeman, C. M.; Islam, M. S.; Jackson, R. A.; Leslie, M.; Tomlinson, S. M. *Philos. Mag.* **1988**, *58*, 123–141.

(35) Dick, B. G.; Overhausear, W. *Phys. Rev. B* **1958**, *112*, 90–103.

(36) Ramsahye, N. A.; Bell, R. G. *J. Phys. Chem. B* **2005**, *109*, 4738–4747.

(37) Dauber-Osguthorpe, P.; Roberts, V. A.; Osguthorpe, D. J.; Wolff, J.; Genest, M.; Hagler, A. T. *Proteins: Struct., Funct., Genet.* **1988**, *4*, 31–47.

(38) Schröder, K. P.; Sauer, J. *J. Phys. Chem.* **1996**, *100*, 11043–11049.

(39) Gale, J. D.; Rohl, A. L. *Mol. Simul.* **2003**, *29*, 291–341.

(40) Le Bail, A.; Duroy, H.; Fourquet, J. L. *Mater. Res. Bull.* **1988**, *23*, 447–452.

(41) Larson, A. C.; von Dreele, R. B. *GSAS Generalized Structure Analysis System, Laur, 86−748*; Los Alamos National Laboratory: Los Alamos, NM, 1994.

(42) Rietveld, H. M. *J. Appl. Crystallogr.* **1969**, *2*, 65–71.

(43) van Koningsveld, H.; van Bekkum, H.; Jansen, J. C. *Acta Crystallogr.* **1987**, *B43*, 127–132.

(44) Park, S. H.; Grobe, R. W.; Graetsch, H.; Gies, H. *Stud. Surf. Sci. Catal.* **1997**, *105*, 1989.

(45) Bhange, D. S.; Ramaswamy, V. *Microporous Mesoporous Mater.* **2010**, *130*, 322–326.

(46) Grau-Crespo, R.; Acuay, E.; Ruiz-Salvador, A. R. *Chem. Commun.* **2002**, 2544–2545.

(47) Baimpos, T.; Giannakopoulos, I. T.; Nikolakis, V.; Kouzoudis, D. *Chem. Mater.* **2008**, *20*, 1470–1475.

(48) Colligan, M.; Forster, P. M.; Cheetham, A. K.; Lee, Y.; Vogt, T.; Hriljac, J. A. *J. Am. Chem. Soc.* **2004**, *126*, 12015–12022.

JP1073736